



ARTICLE

Assessment of Aged Offshore Jacket Type Platforms Considering Environmental Loads and Degradation Parameters

Yazeed Al-Radhi^{1,*}, Farzad Hejazi², Azmi Abdulkarim³ and Ali Feroozi⁴

¹Department of Civil Engineering, Universiti Putra Malaysia, Serdang, 43400, Malaysia

²Housing Research Center, Faculty of Engineering, Universiti Putra Malaysia, Serdang, 43400, Malaysia

³Structural Department, DAR-Energy Sdn. Bhd., Kuala Lumpur, 50400, Malaysia

⁴Faculty of Engineering, University of Botswana, Gaborone, 999106, Botswana

*Corresponding Author: Yazeed Al-Radhi. Email: alradhi_yazeed@yahoo.com

Received: 09 May 2020 Accepted: 25 May 2022 Published: 08 May 2023

ABSTRACT

Offshore steel structures are a common investment in oil and gas industries operating in shallow to medium depth seas. These structures have become increasingly popular since the mid-19th century, with a typical design life of 30-50 years. Despite their popularity, the structural integrity of existing offshore structures remains a controversial topic. Environmental loads and material degradation have been identified as significant factors that can compromise the structural integrity of offshore structures. To address this issue, this study aims to investigate the reserved strength capacity of a selected offshore structure located in the Malaysian Seas. The study will explore the effect of oceanographic data, variations in vertical load, and corrosion on the structure's main members. To determine the impact of each variable on the reserved strength ratio (RSR) of the structure, several pushover analyses were conducted with different variables. Previous literature has shown little or no relationship between seawater wave height, gravity loads, and corrosion allowance on submerged steel members and the RSR of offshore structures. However, this study aims to fill this gap in knowledge by examining these variables' effects on the RSR of offshore structures. The study's findings indicate that even a slight increase in wave height can significantly impact the structure's RSR due to the increase in lateral loading, potentially leading to severe damage to structural components and the foundation model. Additionally, gravity loads had an adverse effect on the RSR of the structure when more than double the vertical load was added. Corrosion allowance was also found to impact the RSR, particularly when assuming significant wall thickness corrosion in primary members. Overall, the findings of this study have important implications for the design and maintenance of offshore structures. The results suggest that engineers and operators should pay close attention to the potential impacts of environmental loads, such as wave height and gravity loads, and material degradation, such as corrosion allowance, on the structural integrity of offshore structures. This information can be used to optimize the design and maintenance of offshore structures, leading to safer and more efficient operations.

KEYWORDS

Assessment; life extension; offshore platforms; platform reserved strength ratio; global ultimate strength analysis



1 Introduction

The number of offshore structures is in continuous increment; the application of offshore structures varies depending on the purpose. There are estimated to be more than 9000 offshore oil and gas structures [1,2]. Out of 7000 existing offshore platforms, 93% are fixed platforms in shallow waters [3]. Offshore structures are considered one of the most challenging tasks to be designed and constructed by engineering [4]. The ageing of offshore platforms is a constant and continuous challenge. Several offshore platforms globally have reached their designed span [5–11]. It is estimated that more than 50% of offshore structures are operating beyond their service span in all of the United Kingdom Continental Shelf (UKCS), Norwegian Continental Shelf (NCS) and the Gulf of Mexico Shelf (CMS) [12,13]. The same is in the Middle East, where more than 70% of 800 platforms have exceeded their design span [14]. Out of 200 offshore operating installations in Malaysia, more than 90% have exceeded their design life [15]. Some alterations may have taken place since the first time the structure was designed and built. The loading pattern (e.g., due to subsidence), the environmental load (e.g., due to waves), and the metrological and oceanographic (metocean) data may have changed since the original design, and the structure may have deteriorated to an unknown extent during decades of harsh weather [16].

Despite the rapid growth in oil and gas for deep water technology, a big production cut comes from relatively old and mostly shallow-water platforms, which are still vital to countries with offshore products. The replacement option of these aged structures entails both operational and technical challenges and expensive solutions [17–19]. Operators and stakeholders are bound by factors about the continuous service of these aged offshore installations, such as enhanced oil recovery production, falling profit margins imposed by the drop in oil prices and uneconomical small field discoveries [3,20]. In common, proper safety could be achieved by implementing the latest compliances rules and regulations in the respective field of expansion. However, it is ambiguous to perform such safety compliance regarding life extension [1,21,22]. A method such as documentation of which structure has reached its design life is not possible using design regulations, even if no cracks have been detected. Hence, it is vital to form a future scheme to present the minimum work to be done to achieve proper structure safety beyond its original design age based on the residual strength the structure presents after the failure of key components [23].

There has been extensive research work to propose recommendations for assessing existing offshore platforms [1,24–31]. Several assessment criteria, such as target reliability levels, consequences of failures, and wave loads, have been addressed. Different analysis levels are proposed within the aforementioned guidelines, such as linear with component check, linear with redundancy, structural reliability, and finally non-linear pushover analysis [26,29,30,32]. Sensitivity analysis is required to address problems about which parameter is most significant for probabilistic analysis [33,34]. This paper aims to investigate three different parameters to evaluate structural integrity through non-linear pushover analysis. These parameters selected are wave height, gravity load and corrosion allowance (thickness reduction) on primary members.

Ultimate strength assessment for offshore platforms, obtained by non-linear pushover analysis, is recognized by higher redundancy since it is built up by components [21,35]. Ultimate strength is dependent on the parameters chosen to be assessed against, which come from technology awareness and industry experience. For instance, Sunder [36] carried out numerical models to assess two platforms sensitivity to variation in wave height, wave period and hydrodynamic force coefficients (C_d & C_m) within the north sea environment. Ultimate strength is also influenced by strength degradation [37], which is led by stiffness loss, differential settlement due to unbalanced loads such as heavy drilling campaigns, fabrication quality, weld failure due to fatigue loads [38] and inadequate structural inspection and maintenance [39]. In regard to the previous investigations, the effect of foundation modelling has been neglected in the response of jacket reserved strength against wave loads. The foundation models were

assumed to be rigid, which this study will aim to fulfill. Platforms' dynamic responses when subjected to variations in soil parameters and pile bottom tip conditions showed a very sensitive relationship with the platform's natural frequency [40]. A significant increase in deck lateral displacement is witnessed for the ductile jacket inclusive of the non-linear pile-soil interaction. However, the effect on the capacity to carry further lateral load is small [41]. Furthermore, the previous studies defined the top mass as a lumped model. In this paper, the top decks are modelled as per real drawings with exact load applications as per obtained details from a local firm, further discussed in [Sections 2 and 3](#).

Moreover, previous studies showed very little details on the impact of varying topside loads with real non-linear foundation model to the platform's reserved strength represented by RSR. Furthermore, very limited details showed the impact of the maximum corrosion allowance applied to the primary members impacting the structure's reserved strength with non-linear foundation model and distributed topside masses. This led to three main motivations for this study: (i) Conduct a sensitivity analysis of a jacket type platform against wave height using a pile-soil interaction (PSI) model, (ii) conduct a sensitivity analysis of a jacket type platform with varying topside loads, and (iii) conduct a sensitivity analysis of a jacket type platform with a reduction in primary members wall thickness representing the minimum corrosion allowances presented in design codes [26,42]. A comprehensive flowchart of this work is summarized in [Fig. 1](#).

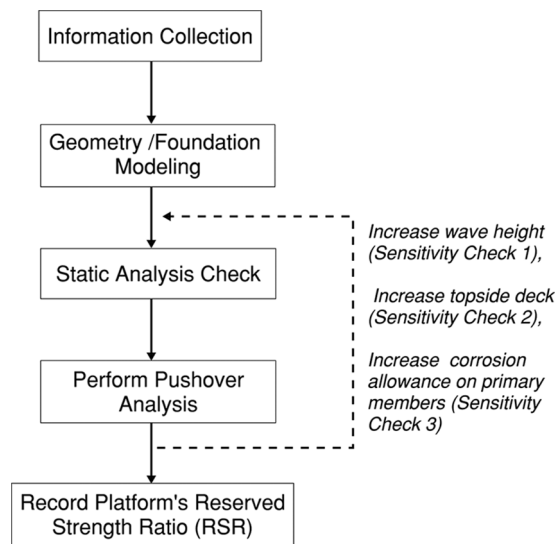


Figure 1: Comprehensive flowchart for conducted study

A detailed flow chart for each task is presented in [Fig. 2](#), which each step is further discussed in [Sections 2–5](#).

2 Geometry and Numerical Modelling

2.1 Geometry

(i) Perform a sensitivity analysis of a jacket type platform against wave height using a pile-soil interaction (PSI) model; (ii) perform a sensitivity analysis of a jacket type platform with varying topside loads; and (iii) perform a sensitivity analysis of a jacket type platform subjected to a reduction in primary member wall thickness representing the minimum corrosion allowances presented in design codes [43] of the ocean environment within the Sabah State. Details of as built survey provided local firm [44] was adopted in the design parameters for environmental conditions. The Metocean criteria were obtained for

the Malaysian coastal areas provided by a local consulting company in Malaysia [43]. The platform used for this study is detailed as follows:

Number of jacket legs	4
Number of Skirt Piles	4
Mudline Elevation (m)	61 (below sea level)
Pile Penetration (m)	95 (below mudline elevations)
Jacket Height (m)	69
Number of Decks	3
Topside Height	47.50 m above mean sea level
Miscellaneous Structure	Helipad, Crane Mounting Support, Dropped object frame, Boatlanding

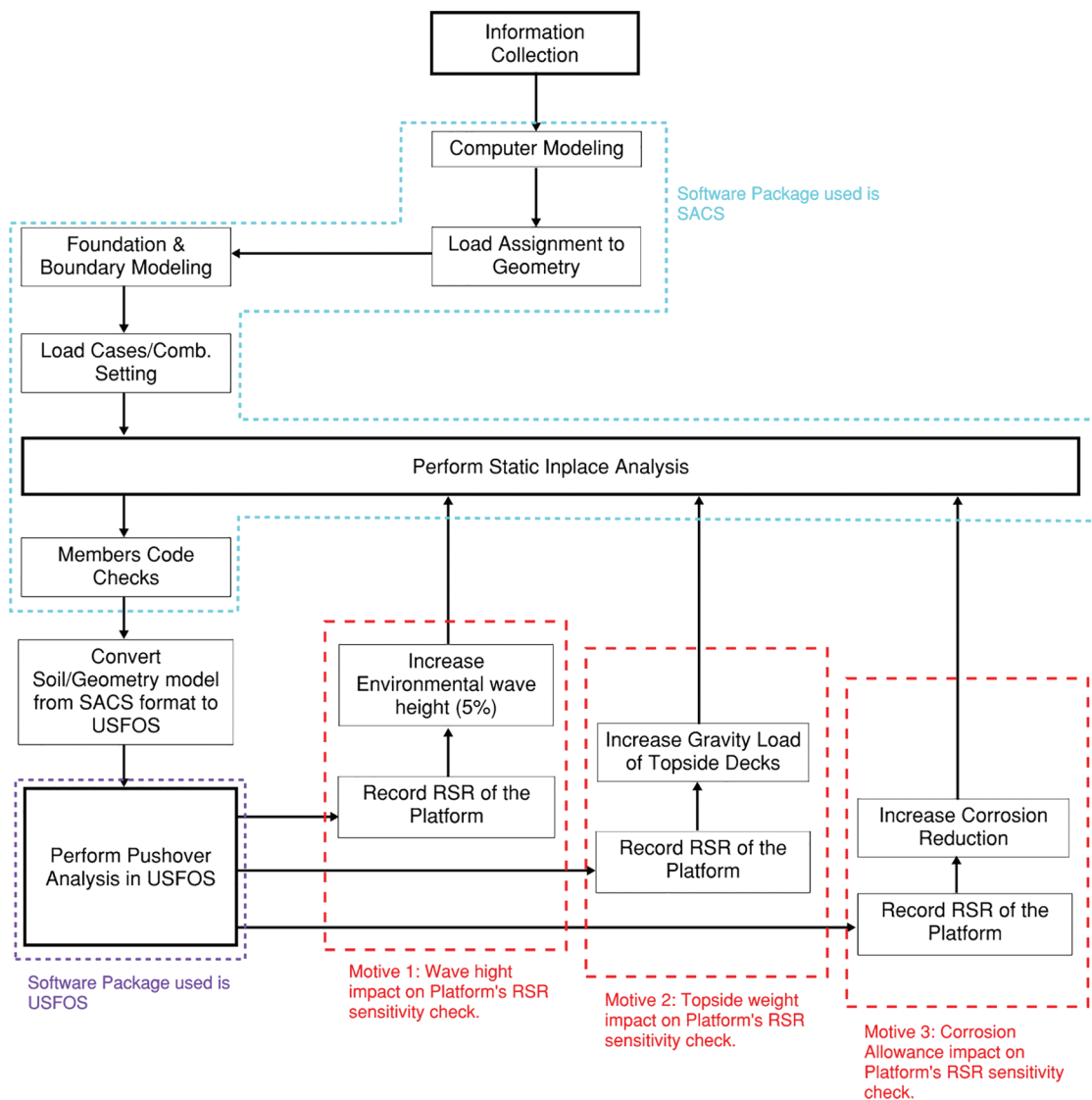


Figure 2: Detailed flowchart for the conducted study

2.2 FEA Modelling

The structure was modelled from proposed structural drawings with applied loads obtained from the same source. The finite element software for the static analysis is SACS [45], a three-dimensional (3D) space frame computer finite element modelling package specializing in offshore structural analysis. The software is versatile in assigning environmental loads such as waves and currents to offshore structures along with other sea environmental parameters per the Metocean criteria. SACS comprises several sub-analysis packages that specialize in a certain type of analysis. Table 1 below summarizes the software components used for the static analysis.

Table 1: SACS computer programs

Component	Analysis
PRECEDE	Interactive modeling and plotting
SEASTATE	Environmental load and mass generation. Combination of basic load cases.
PRE/SOLVE	Static structural analysis
POST	Results reporting and member code checking as per the assigned design code
JOINT CAN	Tubular steel joint checks used for primary circular member connections
DYNPAC	Modal analysis/Dynamic characteristic
WAVE RESPONSE	Dynamic deterministic and random waves analysis
PSI	Pile soil interaction model

The jacket model comprised all jacket members, including legs, diagonal braces, horizontal braces, and piles above the mudline. At work points, members were assumed to be congruent. Brace eccentricities have been introduced based on a 75 mm minimum gap on primary connections. The joint cans and brace stubs were modelled using the member segmenting feature in SACS (JOINT CAN). Mud mats, anodes, walkways, stairs, ladders, and other appurtenances were not modelled for the hydrodynamic force calculation, yet their weight was included under the jacket appurtenances dead loads. Nonstructural members like conductors and risers were modelled with appropriate member end fixities to simulate the actual support to the main frame and ensure the environmental loads obstructed by its surface area are carpentered.

To simplify the analysis and ensure minimum errors, the topside structure was prepared independently and was structurally analyzed. Upon completing a full check of its compliance, it was combined in a full model with the jacket structure where relevant load cases were maintained. A reduction to the primary standing members' submerged thickness was applied to allow for the corrosive environment within the splash zone area at sea level.

Upon modelling and assigning the loads as per Table 2, static structural analysis was performed to get the result of the full model. The basic load cases generally covered the self-weight of the structure, unmodelled dead loads, equipment and piping dead and operating loads, topside open area live loads, and environmental loads (wind, wave and current).

The static model is preceded by a dynamic analysis to obtain both the structural and environmental loads' dynamic equivalent masses and forces to be applied as equivalent loads in an assigned load case. In order to account for the dynamic response of the jacket, a dynamic amplification factor (DAF) was applied using a single degree of freedom dynamic amplification analysis since the structural period was found to be less than 2.5 s. The static and dynamic analysis are not included in this paper, but relevant details are provided where referred to.

The structural analysis was performed using SACS Pre and Solve processors. The analysis was based on a linear elastic response of the structure under static loading conditions. The structure was idealized as a

three-dimensional space frame made of beam-column finite elements with defined boundary conditions. The static analysis gave tabulated joint deflections and member forces and moments for each of the load conditions. The static analysis of the full model with the soil interaction was performed and ensured compliance before proceeding with the non-linear pushover analysis.

For the redundancy analysis or non-linear pushover analysis, the software USFOS [46] was used due to its capability in conducting global non-linear behavior of offshore structures. USFOS is a rigorous Finite Element analysis program suited for indeterminate prismatic structures such as substructures, as it is designed to handle the large number of plastic hinges developed in structural and pile members. It is also capable of tracing system collapse mechanisms accurately.

Unlike linear analysis methods, which can only determine the structural response up to first member yielding, USFOS has the capability to determine the structural response beyond first member failure with the ability to study the elastoplastic behavior of the structure during strain hardening and stress-strain development, hence enabling the system strength to be predicted. The solution strategy deployed for the pushover analysis is to use one finite element per structural element. This allows the use of the FE mesh from the linear analysis, i.e., beam-element formulation but valid for large displacements and restricted to small strains.

Geometrical nonlinearity at the element level is considered by additional second order stress terms. The geometrical non-linearity at a global level is considered by updating the structure's geometry at each load step. Material nonlinearity is described by means of a lumped plastic formulation at the member ends and mid-span. A plastic hinge is inserted in the model each time the cross-sectional load reaches the plastic capacity of that cross-section for combined bending and axial loading. The member cross-section is assumed to remain planar. The yield criterion is expressed in terms of the stress resultants such as axial force, shear force, torsion and bending moment and normalized against the plastic capacities as follows:

$$F_y = f_y(N, M_x, M_y, M_z, s_y, Q_y, Q_z) - 1 = 0$$

This formulation is equated for a cross section in the fully plastic condition as follows:

$$F = \frac{\sqrt{M_x^2 + M_y^2}}{z M_p} - \cos \frac{\pi}{2} \frac{N}{z N_p} = 0$$

where:

$M_p = \sigma_y W_p$ is the plastic bending moment.

$N_p = \sigma_y A$ is the plastic axial force.

And the size of the failure surface is given by the factor z .

As the aim of this work is to investigate the platform response to the offshore load application, the ultimate strength of the platform was assessed by first applying the gravity loads to the ultimate limit as per the real case, followed by incremental load stepping for the lateral environmental loads until a brittle failure was detected by the software. The USFOS analysis procedure used between the static (using SACS) and obtained non-linear pushover analysis is described in the following steps:

1. Basic load cases for operating gravity loads are applied to unity (1.0).
2. Environmental wave load cases (100-year waves) are incrementally applied until a defined characteristic displacement is reached.
3. Each environmental wave loads are applied in predefined steps, i.e., 1%.
4. The deformed nodal coordinates are updated after each load step to record the changes in the geometry.
5. Element stiffness is computed according to the updated geometry and to be re-assembled in each load step.
6. The plastic capacity of the element (end and mid) is checked at each load level and is automatically scaled to the yield capacity whenever the force exceeds the element capacity.

7. As element forces reach to their yield surfaces, a plastic hinge is incorporated to demonstrate the material non-linearity. The plastic hinge is removed when the member later is unloaded and thus becomes elastic.
8. The load increment is automatically reversed if global instability is detected.
9. RSR of the structure is retrieved at the structure's collapse point. RSR is the environmental wave loads (100-year wave) factor applied at the collapsed point.
10. Collapse Base Shear is obtained by multiplying RSR with 100-year Base Shear of a specified direction.
11. The first member failure and final collapse mechanism are identified with their associated load step.

3 Loads

The applied loads varied between permanent loads, variable live loads, environmental loads, and dynamic loads. Permanent loads include the self-weight and equipment weights, while environmental loads include wave, current and wind. Table 2 summarizes the static load cases with the contingency factors applied to the platform, which are obtained from the existing structure in Malaysia [44].

Table 2: Applied static loads to the platform

SACS basic load case	Description	Ref.	Cont. factor	Total load (kN)
1	Topsides structural self weight	1	1.15	-18608.85
2	Topside appurtenances load	2	1.22	-10022.00
8	Architectural weight	2	1.25	-3409.03
27	Bridge dead load	1	1.15	-2168.90
1A	Substructure computer generated dead load	1	1.15	-17983.27
2A	Substructure appurtenances load	1	1.20	-6291.52
2B	Substructure appurtenances buoyancy load	2	1.00	2035.55
3A	Equipment dry weight	2	1.25	-6297.28
4A	Piping dry weight	2	1.25	-1225.75
5	Electrical bulk weight	2	1.25	-2910.36
6	Instrument bulk weight	2	1.25	-1486.53
7	Safety weight	2	1.25	-250.29
20	Crane dead load	1	1.25	-1172.3
11	Lower deck open area live load	3	0.67	-3804.46
12	Main deck open area live load	3	0.67	-3497.17
13	Upper deck open area live load	3	0.50	-1288.13
14	Living quarters open area live load	3	0.70	-10066.91
15	Helideck open area live load	3	1.00	-313.82
16	Laydown area live load-15 kpa	3	1.00	-1106.45
18	Muster area live load-10 kpa	3	0.50	-581.60
28	Bridge live load	2	1.00	-624.00
3C	Equipment hydrotest weight	2	1.25	-3330.5
4C	Piping hydrotest content weight	2	1.25	-306.40

Note: The loads magnitude is obtained from the following references:

1. SACS Software Self-Generated weight.
2. Details of Mechanical, Instrumental, Electrical and Architectural Loads are provided by a local offshore consultant company for a go by project.
3. Pressure loads are based on Petronas Technical Standard [42,47].

The applied environmental loads are included in the analysis based on real data that was provided by an external source. The details of the data include sea wave parameters, sea current speeds, wind speeds, marine growth, salinity of water for corrosion allowance calculation, water depth of the area, and the sea-bed elevation and Metocean Criteria [43].

4 Foundation Modelling

A single SACS PSI was used to model the piles and surrounding soil. SACS [45] software developed by Bentley has the package of PSI (Pile Structure Interaction), which analyzes the behavior of a pile supported structure subject to one or more static load conditions. Finite deflection of the piles (“P-Delta” effect) and non-linear soil behavior both along and transverse to the pile axis are accounted for. The pile model below the pile head will include geometry, sectional and material properties, and length. A pile head joint is defined at the boundary where the linear elastic structure ends, and the elastic pile surrounded by non-linear soil starts. Pile head joints are modeled at mudline elevations. Soil is modeled as non-linear springs unmodeled soil data for the P-Y lateral stiffness, Q-Z bearing capacity, and T-Z friction capacity. The curves for P-Y, Q-Z and T-Z are obtained from the soil report for the proposed platform. The platform is supported on Grids A1, A2, B1, and B2 as shown in Fig. 3 below.

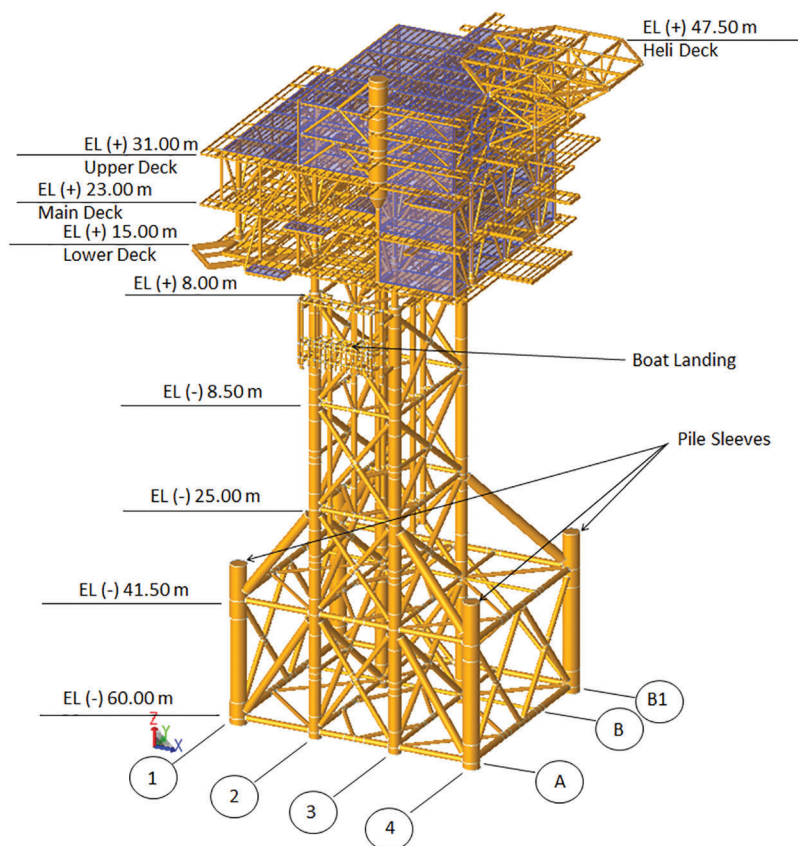


Figure 3: Modeled platform

The details of the soil data are obtained from the geotechnical report for the engineering assessment for the platform, which was provided by an external party to depict the actual properties of the soil where the platform is to be constructed.

The soil profile for the site consists of calcareous clay with intercalated layers of sand and silt. Eleven soil units have been identified to a depth of 100 m. The division into units is derived from a geotechnical perspective for foundation engineering purposes. Soil profile is described as per As-Built Survey [48] as below:

Description	Depth (m)
Calcareous CLAY, very soft, olive grey with few shells and shell fragments.	0–2
Calcareous CLAY, firm to stiff, olive grey with partings, laminations and seams of silt and fine sand, traces of organic matter.	2–12
Calcareous Silica SAND, dense to very dense, medius dark grey, locally gaseous.	12–15
Calcareous CLAY or SILT, very sandy, stiff to very stiff, olive grey, with many seams and layers of silt and fine sand, locally gaseous.	15–34.5
Calcareous CLAY, stiff to very stiff, olive grey with partings, laminations and seams of find silly sand, locally gaseous.	34.5–50
Calcareous silica fine SAND, dense to very dense, olive grey to olive black, locally with seams of clayey shell debris.	50–53.5
Calcareous CLAY, very stiff, olive grey, with partings and laminations of silt, locally layer of sand.	53.5–67
Calcareous silica SAND, dense, olive grey, with mica, with laminations of silt and shell fragments.	67–70
Calcareous sandy CLAY, very stiff to very hard, olive grey with partings and laminations of silt, locally a layer of sand.	70–81
Calcareous silica SAND, dense, olive grey to olive black, with laminations of silt.	81–94

5 Pushover Analysis

USFOS [46] is used for this task since it is suited for indeterminate prismatic structures such as substructure as it is designed to handle a large number of plastic hinges developed in structural and pile members. The solution strategy deployed for the pushover analysis is to use one finite element per structural element. This allows the use of the FE mesh from the linear analysis, i.e., beam-element formulation but valid for large displacements and restricted to small strains. Material non-linearity is described by means of a lumped plastic formulation at the member ends and mid span.

As elaborated in Section 2.2, the model is originally obtained from SACS software, from which both the geometry and foundation model are converted to USFOS using a third converter software (STRUMAN). A check was conducted to ensure the conversion was correct by running a static analysis in USFOS and checking the resulted loads and reactions and comparing them with the original model from SACS prior to proceeding to wave non-linear pushover analysis. The wave pushover analysis is conducted for several wave attack directions, which are postulated in Fig. 4. The load combination consists of the applied static (gravity) load associated with the wave, current, and wind loads. The maximum wave height used for the analysis is 9.8 m for 1-year operating and 15.8 m for 100-year storm conditions.

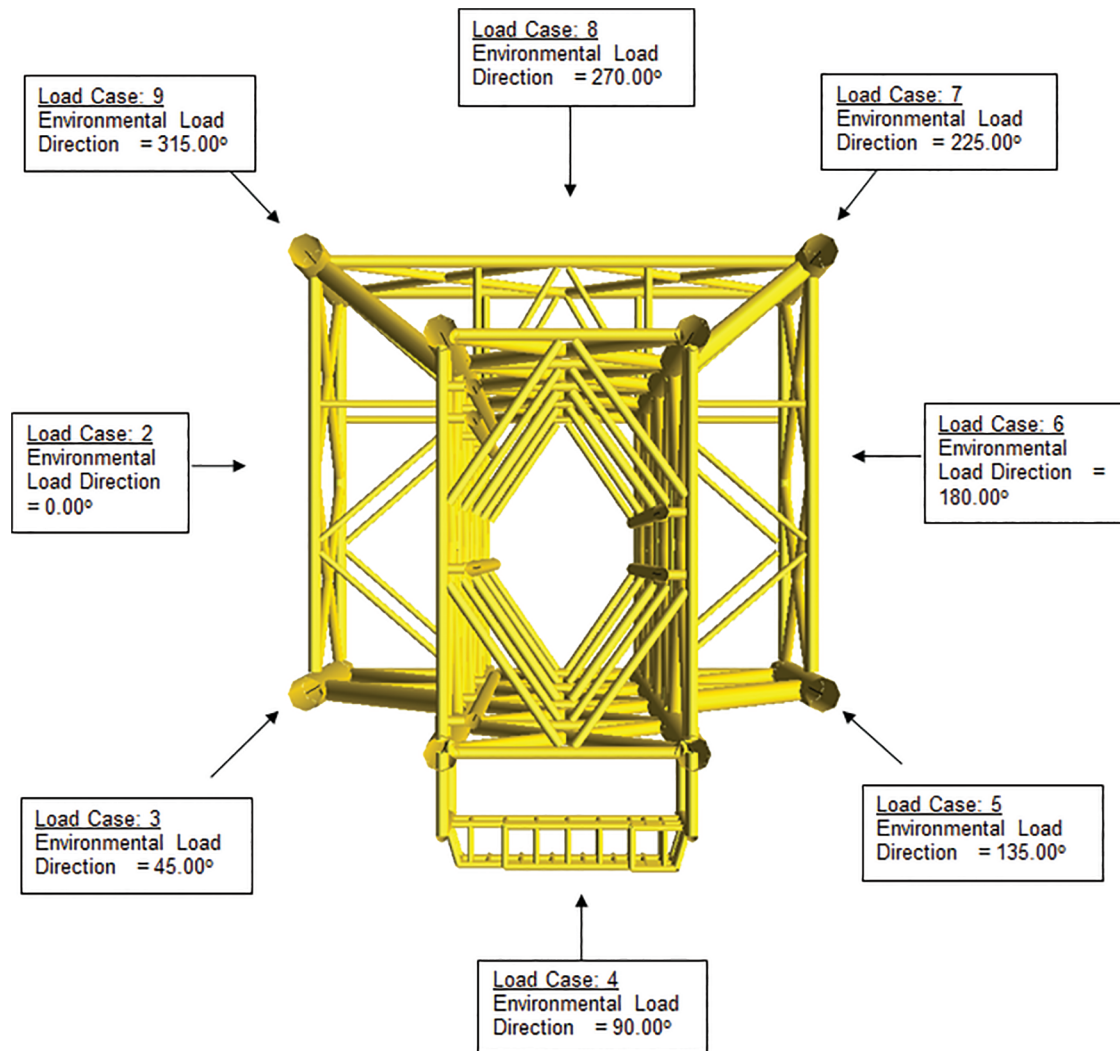


Figure 4: Applied environmental load directions

The study considered eight (8) directions for two reasons. The first is to investigate which direction results in the maximum base shear depending on the platform configuration and weakest axis of the structure, while the second reason is due to the provided metocean data with different wave height and period at each direction. [Table 3](#) below lists the platform direction with corresponding extreme environmental data. The dynamic behavior of the structure was also considered by running a simplified dynamic analysis in order to generate the platform dynamic amplification factor for the wave and current inertia loads on the structure.

Table 3: Extreme environmental directional data

Parameter	Direction							
	N (0°)	NE (45°)	E (90°)	SE (135°)	S (180°)	SW (225°)	W (270°)	NW (315°)
Wind speed (m/s) 1-h mean	31.3	30.6	27.5	22.8	21.9	26.8	26.2	30.5
Significant wave height, Hs (m)	9.0	7.0	5.3	4.2	4.3	6.8	7.0	9.9
Zero crossing period, Tz (s)	8.2	7.7	7.0	6.4	6.5	7.7	7.7	8.3

(Continued)

Table 3 (continued)								
Parameter	Direction							
	N (0°)	NE (45°)	E (90°)	SE (135°)	S (180°)	SW (225°)	W (270°)	NW (315°)
Peak period, T_p (s)	13.7	11.9	10.3	9.0	9.1	11.8	12.0	14.5
Max wave height, H_{max} (m)	14.3	11.2	8.5	6.7	6.8	11.0	11.3	15.8
Associated period, T_{ass} (s)	10.7	10.1	9.2	8.4	8.4	10.1	10.1	10.8

6 Analysis Scenario

The main objective of this study is to investigate the effect of the environmental loads on the platform's RSR. The environmental effects and gravity loads are the main parameters whose effects on platform RSR are being investigated. The analysis was conducted using two software packages, SACS & USFOS where the analysis procedure is discussed in Sections 2–4 of this study. Upon obtaining the converted model in USFOS, the topside weight effect is studied by incrementing the weight in several trials and recording the platform RSR by running a wave non-linear pushover analysis for each trial. For this study, only operating waves are used to record the RSR as the aim of the study is to determine the effect of loading on the platform's reserved capacity.

The other parameter, which is the main parameter, is the wave height and period effect on the platform RSR. The wave height is increased by 10% for several trials until the platform collapses, where the operating wave is used as the bench starting parameter to record several RSR before collapsing. The third parameter that was investigated is the corrosion effect on the platform. The corrosion was modelled as a reduction in the main legs' thickness. Only primary legs and diagonal members were selected for this parameter. The consequence of the analysis in the summary is obtaining the platform RSR by running several runs for wave non-linear pushover analysis. The analysis for the wave height and period effect is studied for each direction (total 8) to determine the weakest jacket response to each direction and based on that, the other parameters were done only for the direction that results in the minimum RSR.

The number of wave non-linear pushover analyses conducted is 96 analyses for the wave height and period, 21 for topside, 8 for corrosion allowance, for a total of 106. As a preliminary test, the model was generated from the structural drawings based on the sizes and configurations specified. A simple static analysis was conducted in order to ensure the platform was intact before running the non-linear analysis. The static analysis was based on AISC 360-10 (2010) [3], as recommended in API RP 2A WSD [26] for the specification of steel structures. Other details for the loading or the design of offshore structures are determined from ISO 2394 (1998), ISO 13822 (2000), ISO 1990 (2002), ISO 19902 (2004), and ISO 19902 (2007) [29,30,49–51].

7 Wave Height and Period Effect on Platform RST

The static wave analysis is obtained as per the applicability of the apparent wave period T_{app} , specific wave height H and storm water depth d in reference to API RP 2A [26]. The wave load is calculated based on Stokes wave theory as per API RP 2A [26]. Stoke's second-order wave components (1st & 2nd) are adopted to provide the steeper and shallower trough. The following formulas represent different components for Stoke's second order wave theory. The dynamic wave pressure adopted as per API RP 2A [26] adopts member wave pressure as follows:

1st Order component:

$$p = \rho g \frac{H \cosh ky}{2 \cosh kd} \cos[k(x - ct)]$$

2nd Order component:

$$p = \frac{3}{4} \rho g \frac{\pi H^2}{L} \frac{1}{\sinh 2kd} \left[\frac{\cosh 2ks}{\sinh^2 kd} - \frac{1}{3} \right] \cos 2(kx - \omega t) - \frac{1}{4} \rho g \frac{\pi H^2}{L} \frac{1}{\sinh kd} [\cosh 2ks - 1]$$

where:

ρ = fluid density.

g = gravitational acceleration.

H = wave height (crest to trough).

$k = 2\pi/\lambda$.

$y = Y$, vertical co-ordinate in frame fixed in bed.

d = crest depth.

x = horizontal co-ordinate in frame moving with wave crest.

c = wave speed.

t = time = water depth.

s = momentum flux per unit span perpendicular to flow.

$\omega = \frac{z}{2k}$, Dummy variable.

The wave height and wave period are increased by 10% of the original value taken from metocean data. The analysis is run until the RSR value for at least one direction reaches a value smaller than 1. This indicates that the structure collapsed before applying the 100% load. Table 4 summarizes the wave input data for the platform's RSR response due to wave effect. The maximum increment is 250% of the original input where a value of less than one (1) is spotted from the direction of 0°. Fig. 4 demonstrates the value of the RSR at each direction with different wave and current input.

Table 4: Applied wave height and period

Increment	Input	Wave height (m) & Wave period (s)							
		0°	45°	90°	135°	180°	225°	270°	315°
0%	Wave height	9.80	9.80	9.80	9.80	9.80	9.80	9.80	9.80
	Wave period	9.80	9.80	9.80	9.80	9.80	9.80	9.80	9.80
	Platform RSR	7.35	7.96	9.14	8.81	8.18	9.80	10.29	9.54
10%	Wave height	10.78	10.78	10.78	10.78	10.78	10.78	10.78	10.78
	Wave period	10.78	10.78	10.78	10.78	10.78	10.78	10.78	10.78
	Platform RSR	6.47	7.06	7.78	7.73	6.97	8.32	8.46	8.06
20%	Wave height	11.76	11.76	11.76	11.76	11.76	11.76	11.76	11.76
	Wave period	11.76	11.76	11.76	11.76	11.76	11.76	11.76	11.76
	Platform RSR	5.61	6.13	6.58	6.64	5.90	6.98	7.00	6.81
30%	Wave height	12.74	12.74	12.74	12.74	12.74	12.74	12.74	12.74
	Wave period	12.74	12.74	12.74	12.74	12.74	12.74	12.74	12.74
	Platform RSR	4.87	5.31	5.54	5.72	5.01	5.86	5.85	5.78

(Continued)

Table 4 (continued)									
Increment	Input	Wave height (m) & Wave period (s)							
		0°	45°	90°	135°	180°	225°	270°	315°
40%	Wave height	13.72	13.72	13.72	13.72	13.72	13.72	13.72	13.72
	Wave period	13.72	13.72	13.72	13.72	13.72	13.72	13.72	13.72
	Platform RSR	4.20	4.61	4.72	4.87	4.28	4.97	4.94	4.91
50%	Wave height	14.70	14.70	14.70	14.70	14.70	14.70	14.70	14.70
	Wave period	14.70	14.70	14.70	14.70	14.70	14.70	14.70	14.70
	Platform RSR	3.59	4.04	4.02	4.17	3.65	4.25	4.18	4.17
60%	Wave height	15.68	15.68	15.68	15.68	15.68	15.68	15.68	15.68
	Wave period	15.68	15.68	15.68	15.68	15.68	15.68	15.68	15.68
	Platform RSR	3.08	3.52	3.44	3.57	3.12	3.63	3.56	3.57
70%	Wave height	16.66	16.66	16.66	16.66	16.66	16.66	16.66	16.66
	Wave period	16.66	16.66	16.66	16.66	16.66	16.66	16.66	16.66
	Platform RSR	2.67	2.99	2.95	3.07	2.69	3.14	3.06	3.09
80%	Wave height	17.64	17.64	17.64	17.64	17.64	17.64	17.64	17.64
	Wave period	17.64	17.64	17.64	17.64	17.64	17.64	17.64	17.64
	Platform RSR	2.25	2.64	2.56	2.62	2.29	2.67	2.62	2.63
90%	Wave height	18.62	18.62	18.62	18.62	18.62	18.62	18.62	18.62
	Wave period	18.62	18.62	18.62	18.62	18.62	18.62	18.62	18.62
	Platform RSR	1.98	2.25	2.23	2.29	2.02	2.34	2.29	2.31
100%	Wave height	19.60	19.60	19.60	19.60	19.60	19.60	19.60	19.60
	Wave period	19.60	19.60	19.60	19.60	19.60	19.60	19.60	19.60
	Platform RSR	1.74	2.00	1.96	2.00	1.75	2.05	2.01	2.02
150%	Wave height	24.50	24.50	24.50	24.50	24.50	24.50	24.50	24.50
	Wave period	24.50	24.50	24.50	24.50	24.50	24.50	24.50	24.50
	Platform RSR	0.96	1.06	1.05	1.08	0.95	1.11	1.07	1.08

Table 3 is represented by a spider plot where each corner represents the direction considered for the wave height and period. The vertical is the platform RSR. Each direction has the resultant RSR value from the conducted pushover analysis at each specified direction as discussed in Section 4. The results are for all the increments from 0% (with normal environmental loads) until 150% of the applied loads. Increments started with 10% increment until 100%, then the range was increased to 50%, where at the first trial, the minimum RSR value was spotted. The minimum RSR value is 0.956, which hits at 0° direction.

The 0° direction is therefore considered the direction that will impose the maximum wave forces on the structure. Fig. 4 illustrates the results of the RSR due to the wave loading effect for each direction. While Fig. 5 shows the relationship between the increase in the wave height and the period against the platform RSR. The collapse wave height (150%) observed in the final step is not realistic, as the wave-in deck would occur on topside modules, which will be another design criterion to be considered in the earlier design stage. It can be seen in Fig. 5 that the direction of 0 degree is the most severe direction that will impose the maximum wave loading on the platform.

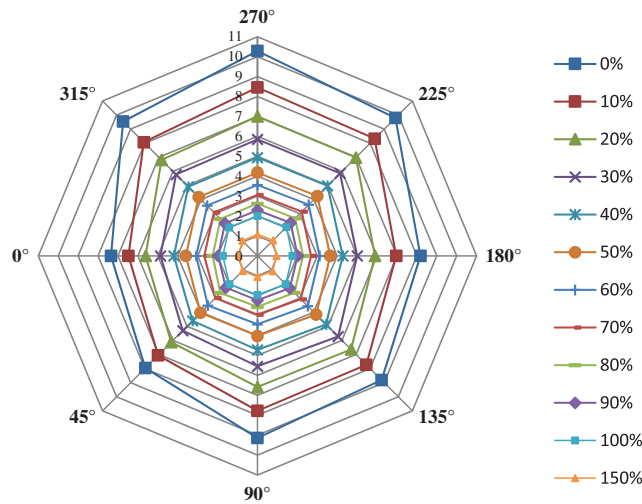


Figure 5: Platform RSR values corresponding to wave height and wave period effect for each direction

As shown in Fig. 6, once the wave height increases, the loading imposed on the structure from the wave will be more. When the wave height increases, the lateral loads and wave dynamic forces on the structure increase significantly, leading to a larger base shear and overturning moment, where platform RSR is dependent on the platform base shear during damaged conditions relative to the normal base shear. The increment has reached 2.5 times the height of operating waves, categorized as a breaking wave per API RP 2A. However, it was assumed to happen to maximize the forces on the structure for the severity study. The overall platform depth is 58.77 m, indicating that not a major wave load is applied at the normal wave height, and that is why it required several load steps (until 250% increment) to reach a significant failure. The 250% wave height is 25.50 m which is very high and impossible to happen as the provided metocean data for 1000-year return wave data is smaller than this value. The maximum 1000-year return period wave height is 15.90 m which is smaller than the 25.50 m wave height unless a non-expected natural event such as a hurricane has occurred.

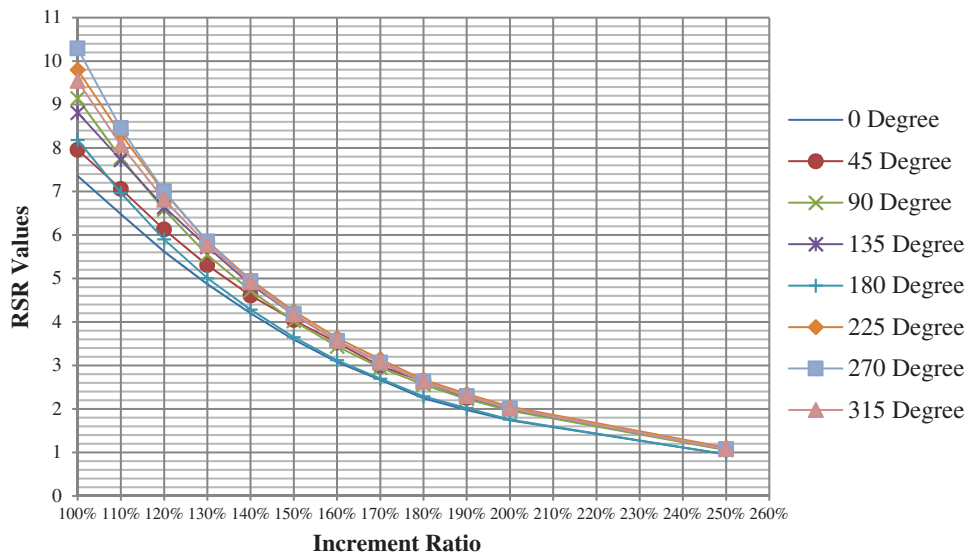


Figure 6: Platform RSR response during environmental wave increment

The results above show that the platform's RSR behaves inversely with the applied environmental waves, where the larger the wave height, the lower the platform's reserved strength ratio (RSR). Based on this conclusion, the structure showed a very stiff response to wave height increment and has collapsed at a very high wave height such that the probability of it happening is very small. Moreover, the figures above prove the theory of the contradictory relationship between the environmental load and platform RSR, where once the wave height increases, the platform RSR decreases. Fig. 7 shows the structure's overall member plastic utilization during the 150% increment in the 0° direction.

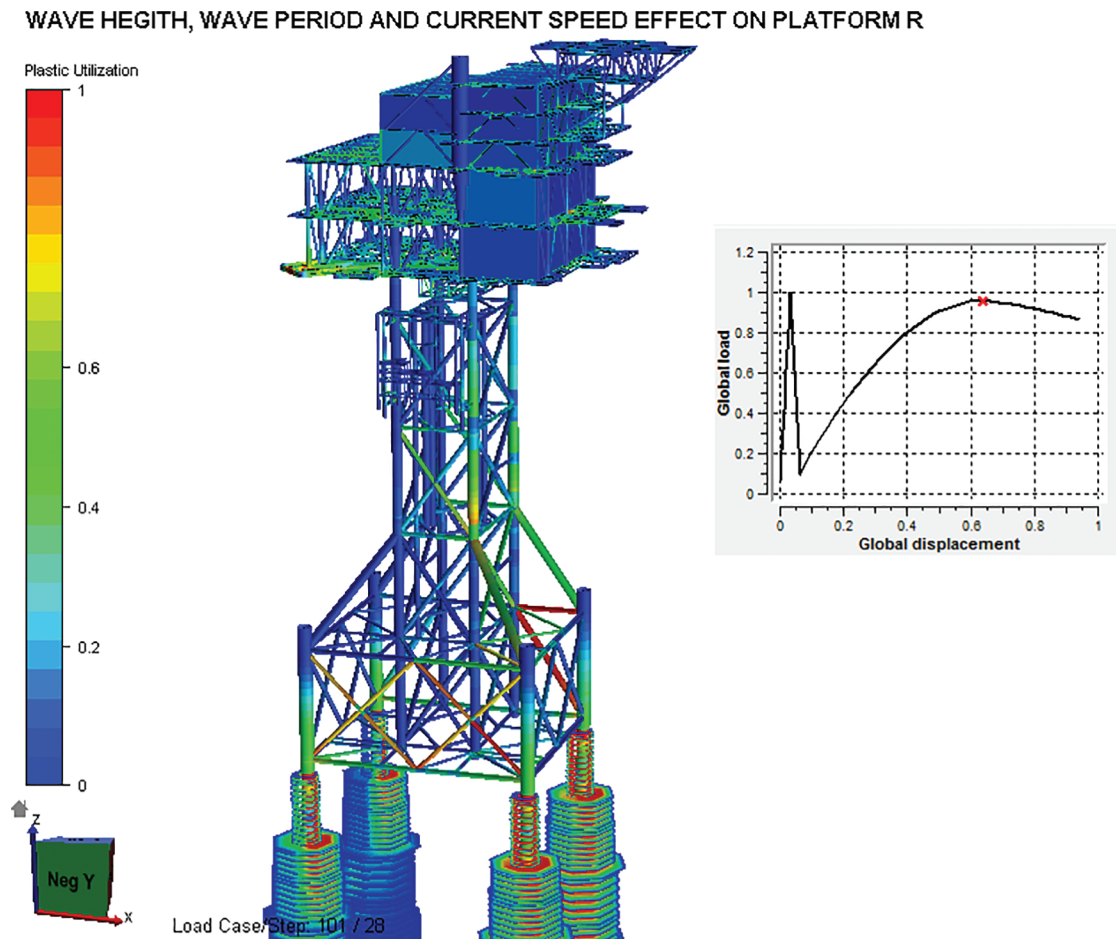


Figure 7: Platform RSR during 250% increment at 0° direction

Through visual inspection of the plastic plots, the platform was witnessed to be overstressed in soil, as the soil is represented by a non-linear spring with the soil properties from the soil report and represented in Fig. 7 by discs with different diameters (the larger the diameter, the stiffer the soil properties at that depth), followed by major structural failure at the members in the lower part of the jacket. The red color in the figure indicates a full utilization of the member cross-section. The graph at Fig. 6 illustrates the structure's load-displacement relationship when subjected to the incremented wave height. The figure shown is only for the latest increment where the structure achieved the minimum RST of 0.96, which is lower than 1.0. The failure of the structure is determined by the drop of the curve in the load-displacement graph, as the curve shows the elastic and plastic behavior of the structure and stops at the rupture point where the

USFOS software terminates the analysis automatically. The rupture point is achieved when several key components of the structure are fully plastic, and no further residual strength has remained.

8 Topside Weight Effect on Platform RSR

On the other hand, and apart from environmental loads, another investigation was conducted on the platform RSR concerning topside weight. Topside weight is defined separately in the analysis by defining it in a separate load combination. The details of the topside weight are shown in [Table 5](#) below. The methodology in this analysis is to increase the factor times the load combination designated for the topside until the platform RSR reaches a value below one (1). The analysis was done with environmental loads (wave, current, and wind) only from one direction, which is the 0° direction, as it was seen in [Section 6](#) that the environmental loads from this direction produce the minimum platform RSR. The total topside weight is 62410.23 kN (6362 MT), including operating and live load, which was assumed to be active during the wave non-linear pushover analysis.

Table 5: Applied topside weight

No.	Load description	Base load (kN)	Cont. factor	Code factor	Total factor	Factored load (kN)
1	Topside computer-generated dead load	-16181.61	1.150	1.000	1.150	-18608.85
2	Topsides appurtenances load	-8214.75	1.220	1.000	1.220	-10022.00
8	Architectural weight	-2727.22	1.250	1.000	1.250	-3409.03
27	Bridge dead load	-1886	1.150	1.000	1.150	-2168.90
10	Sub-lower deck open area live load (7.5 kPa)	-475.34	0.667	1.500	1.000	-475.36
11	Lower deck open area live load (7.5 kPa)	-3804.27	0.667	1.500	1.000	-3804.46
12	Main deck open area live load (7.5 kPa)	-3497	0.667	1.500	1.000	-3497.17
13	Upper deck open area live load (10 kPa)	-1717.5	0.500	1.500	0.750	-1288.13
14	Living quarters open area live load	-6711.27	1.000	1.500	1.500	-10066.91
15	Blanket load at helideck	-209.21	1.000	1.500	1.500	-313.82
16	Blanket load at laydown area (15 kPa)	-737.63	1.000	1.500	1.500	-1106.45
18	Blanket load at muster area (10 kPa)	-775.47	0.500	1.500	0.750	-581.60
28	Bridge live load	-416	1.000	1.500	1.500	-624.00
907	Equipment hydro-test weight	-2697.63	1.250	1.500	1.875	-5058.06
910	Piping hydro-test content weight	-245.74	1.250	1.500	1.875	-460.76
21	Crane live load with dynamic	-490.5	1.000	1.500	1.500	-735.75
26	Helicopter take-off weight (S92)	-126	1.000	1.500	1.500	-189.00
					Total	-62410.23

Figs. 8–10 below illustrate the graph for the jacket RSR response to the topside weight increment. The increments started with the original applied load as detailed in Table 2 and were incremented by 10% at each run, then wave non-linear pushover analysis was performed. The analysis showed that as long as the topside or gravity weight increases, the structure's RSR is not affected much as the RSR mainly depends on the lateral forces. Though the RSR has decreased significantly when the increment has reached 200% of the initial load, the reason for that is the high member failures and stresses from the gravity load where these members are primary members and play a significant role in the structure's stability.

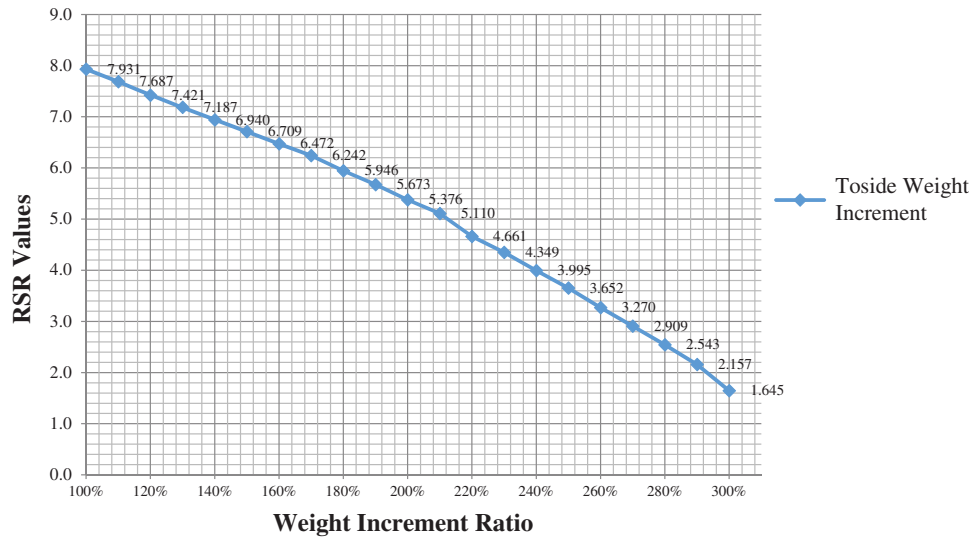


Figure 8: Topside weight and RSR relationship

The topside weight was increased to a maximum factor of 3, and the structure's RSR value is 1.645, which is still above one and safe. A further increase will impose a small reduction in the structure's RSR but significant failures in members who are not the main bones of the structure's stability. Fig. 11 shows the structure member failure and plastic utilization due to topside weight.

Results show that the failure hits the structure before the soil. The soil has shown a very stiff response to the weight increment even though the stress is gravitational. As shown in Fig. 8, the gravity load is increased to the targeted value and released when the full load is achieved. Once the first load is removed, but its effect remains, the next load combination, which represents the environmental load from 0° direction, is applied incrementally until it is either achieved or at least one member fracture is spotted. In the maximum case (factor of 3), the structure has managed to sustain the full environmental load when three times the original topside weight is applied to it. Within this summary, the scenario of the structure's RSR response to gravity load has met the expectations. Once the gravity load increases, the platform RSR will be decreased.

9 Corrosion Effect on Platform RSR

The next parameter investigated in this study is the corrosion effect on the platform reserved strength ratio (RSR). Corrosion is a fundamental parameter that is worth investigating. The best methodology for representing the corrosion phenomena is by applying for corrosion allowance in the model by introducing a reduction in the thickness of the tubular (since all the jacket members are tubular). The reduction was made in an incremental method to observe the effect on the platform RSR. Only primary members were selected for this reduction since these members are the main legs. Table 6 shows the platform RSR corresponding to the reduction percentage. The analysis was done only from the 0° direction as it was

observed to generate the minimum RSR. The reduction was made consistent as it starts with a 5 mm reduction and continues with 5 mm increments until the structure shows significant instability.

WAVE HEIGHT, TOPSIDE WEIGHT EFFECT ON PLATFORM RSR

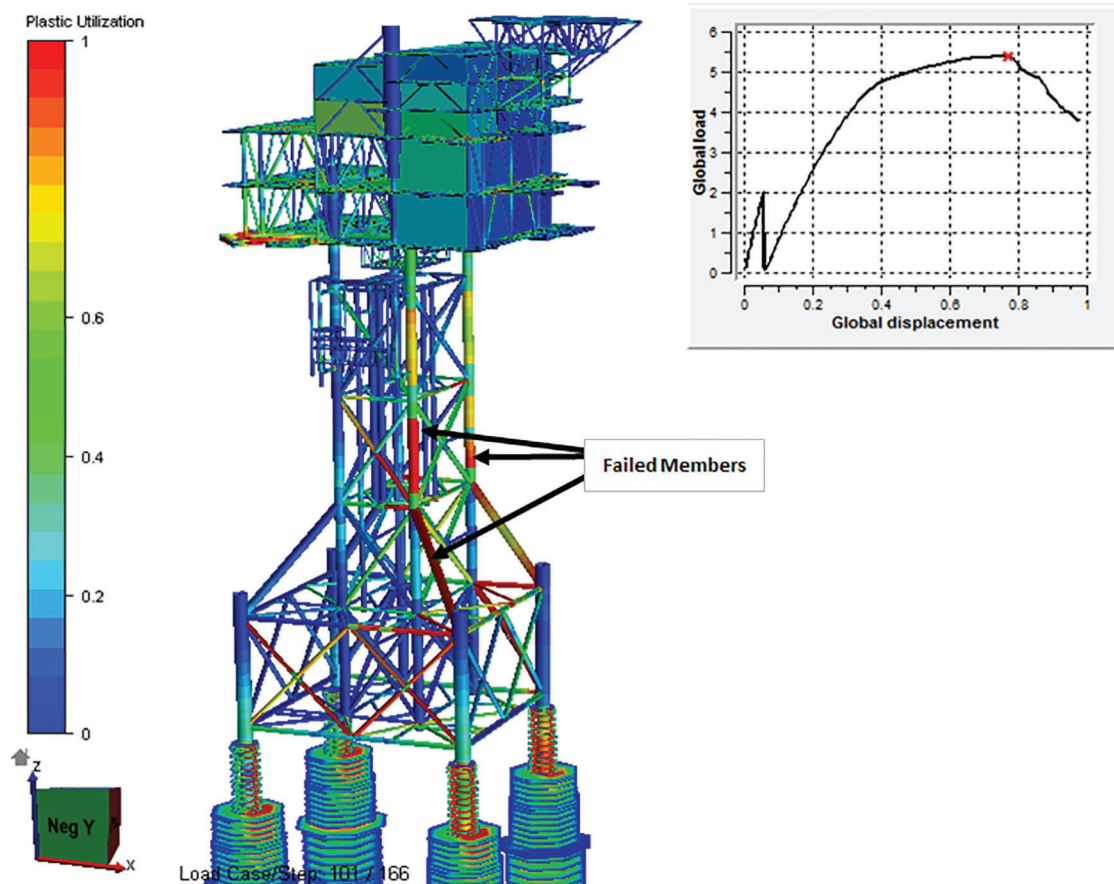


Figure 9: Member utilization failure when 200% of topside weight applied

The first results are almost the same since the overall loading remains the same and the stiffness is not majorly affected by the thickness reduction. Once the reduction is 25 mm in the thickness of the primary legs, the structure significantly decreases the RSR. The reason is that since most of the primary legs have a thickness of 40 mm and this reduction represents 63%, in a simple logical explanation, it will reduce the structure leg stiffness by an equivalent percentage. The structure shows great instability in the subsequent reduction, where it ended up with 35 mm and a corresponding RSR of 0.619. Fig. 11 shows the relationship of RSR with the thickness reduction in primary legs.

The graph proves the concept of the different relationships between the platform RSR and its stiffness. The drastic decrease happens when a significant reduction occurs at 20 mm and forward, as shown in the figure above. Figs. 12 and 13 show the member plastic utilization for the 25 and 35 mm reductions, respectively.

WAVE HEGITH, TOPSIDE WEIGHT EFFECT ON PLATFORM RSR

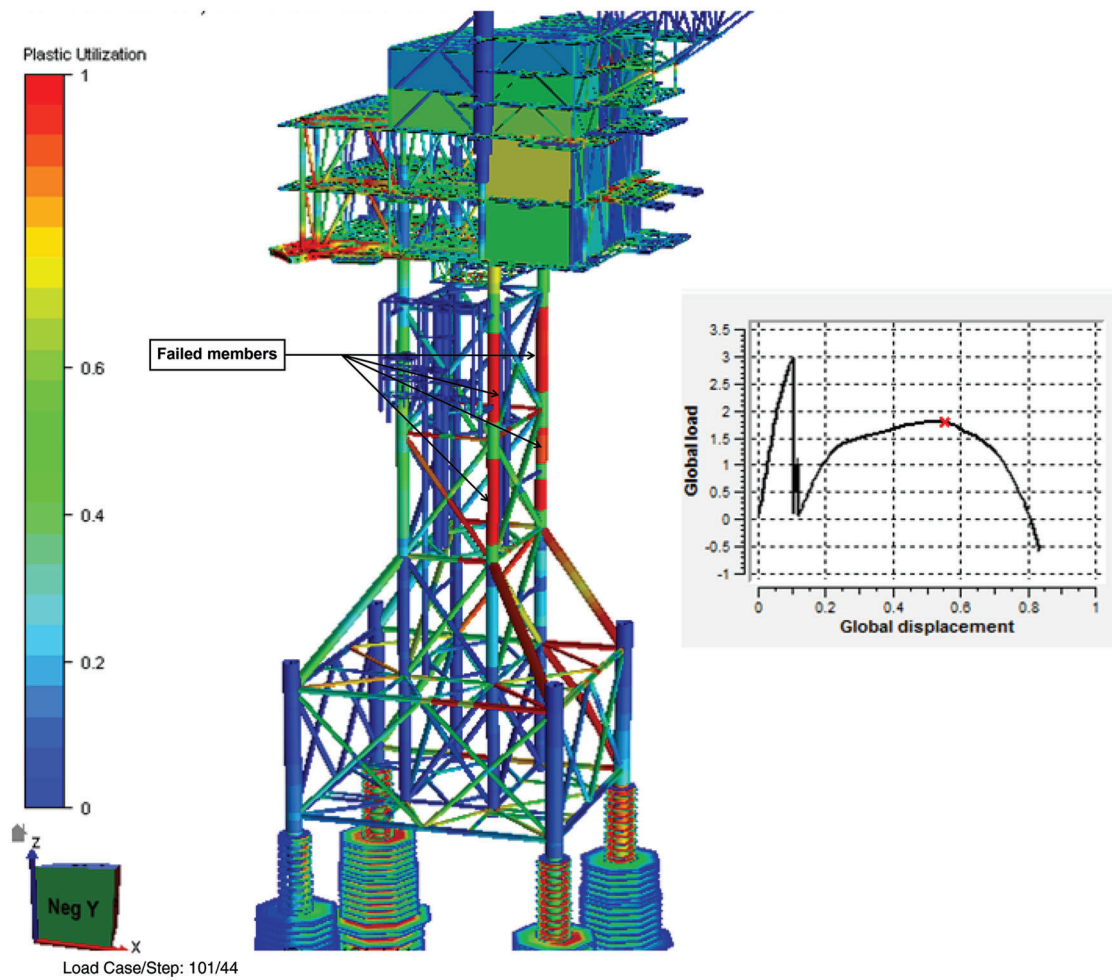


Figure 10: Member utilization failure when 300% of topside weight applied

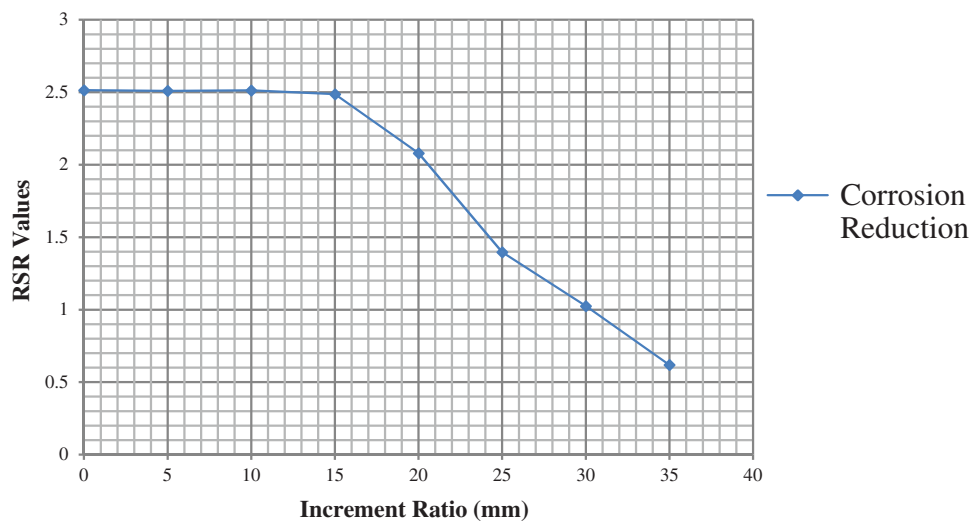


Figure 11: Member corrosion allowance with platform RSR relationship

Table 6: Corrosion allowance and resulted RSR

Corrosion increment (mm)	RSR value
5	2.514
10	2.510
15	2.513
20	2.487
25	1.397
30	1.025
35	0.619

CORROSION ALLOWANCE EFFECT ON PLATFORM RSR

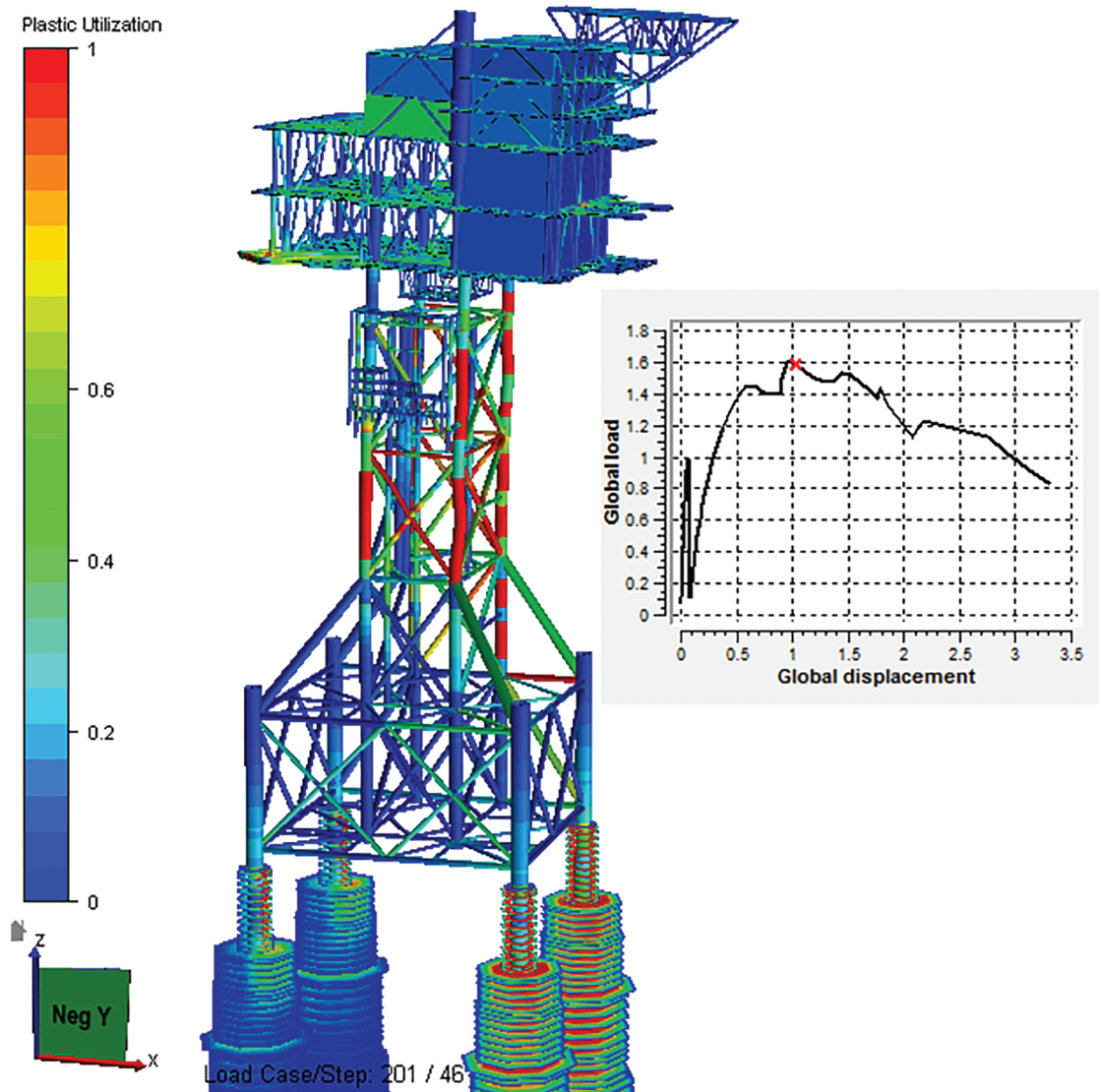


Figure 12: Member plastic utilization for 25 mm

CORROSION ALLOWANCE EFFECT ON PLATFORM RSR

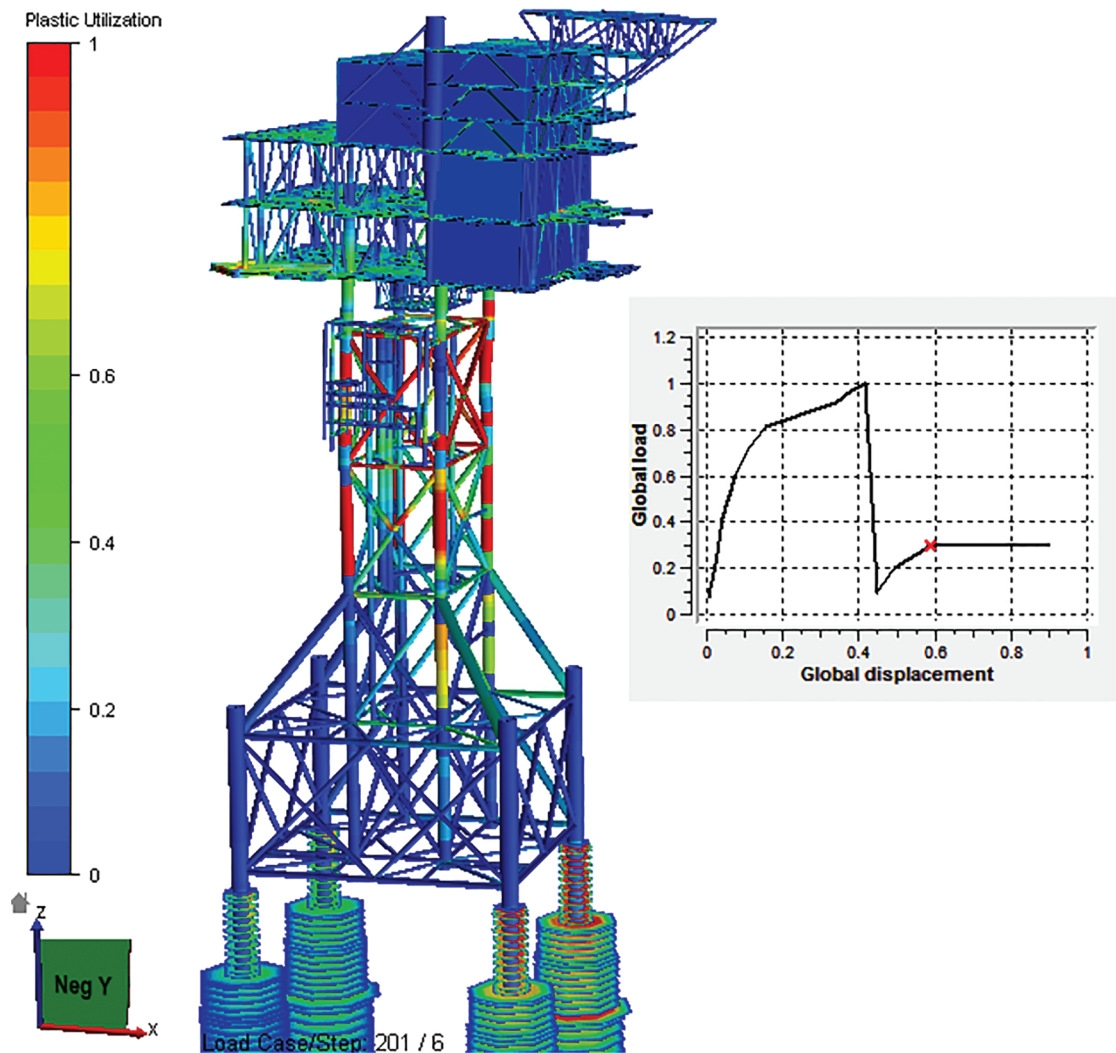


Figure 13: Member plastic utilization for 35 mm

10 Conclusion

This study aims to assess the existing offshore structures through wave non-linear pushover analysis under various conditions. The study was represented by a structure modelled with supplied details from a consulting company in Malaysia in offshore engineering. The model consists of a four-legged platform with four pile sleeves connected to it.

To obtain a direct relationship, the study investigated the environmental loads on the structure's reserved strength ratio (RSR). The study also included the platform RSR relationship with the gravity load increment that could happen over the life span of the platform. The platform RSR decreases with a significant change in the gravity load. Corrosion on steel members in harsh corrosive environments is another major environmental factor affecting platform strength degradation. The maximum wave height reported by the minimum RSR was at an increment of 150% of the original value corresponding to direction 0, with a wave height of 24 m which is unrealistic.

It is concluded that pushover analysis (global ultimate strength analysis) showed that the wave height and period are the most affecting factors in reducing the structure's ultimate strength ratio (RSR). The greater the wave height, the lower the RSR, despite the low occurrence probability.

The structure's topside weight had little effect on its reserved strength ratio (RSR) unless it was 200% or 300% greater than its initial value. At that point, the RSR would be significantly affected due to the structure's stiffness loss, which only occurred during a large increase in the structure's gravity load. In this case, the structure may experience pre-failures for major structural members before the collapse of the structure.

Corrosion on offshore structures is a significant ageing factor at a high level. The structure's RSR is significantly reduced with high levels of corrosion. The critical amount of corrosion that leads to a major failure is spotted at 20 mm. This value is quite high as most applicable design codes call for [26,47] specifying a maximum value of 6 mm for extreme designs on primary members.

Moreover, the offshore structures are mainly affected by the wave forces more than any other parameter. The wave loads are majorly contributing to overturning the structure to the collapse position, where the RSR is majorly reduced.

Acknowledgement: My gratefulness expression goes to my wife and my parents, to whom I owe life-long gratitude for their continuous support. I also express my sincere gratitude to my supervisor Assoc. Prof. Farzad Hejazi for his guidance and encouragement throughout this study. I also express my gratitude to Petrofac-RNZ Engineering Services Sdn. Bhd. for supporting this research study.

Funding Statement: The authors received no specific funding for this study.

Conflicts of Interest: The authors declare that they have no conflicts of interest to report regarding the present study.

References

1. Abdel Raheem, S. E., Abdel Aal, E. M., Abdel Shafy, A. G., Fahmy, M. F., Omar, M. (2021). In-place analysis for structural integrity assessment of fixed steel offshore platform. *Arabian Journal for Science and Engineering*, 46(5), 5031–5045. <https://doi.org/10.1007/s13369-020-05200-3>
2. Gur, T., Choi, J. W., Soyoz, S., Abadie, R. J., Barrios, A. C. (2009). Assessment of platform cognac using instrumentation data. *Offshore Technology Conference*, Houston, Texas.
3. Aeran, A., Siriwardane, S. C., Mikkelsen, O., Langen, I. (2017). A framework to assess structural integrity of ageing offshore jacket structures for life extension. *Marine Structures*, 56, 237–259. <https://doi.org/10.1016/j.marstruc.2017.08.002>
4. Walker, A. C., Ellinas, C. P., Snedden, W. (1997). Use of structural simulation for extension of life of offshore structures. *The Seventh International Offshore and Polar Engineering Conference*, Honolulu, Hawaii, USA.
5. Ersdal, G. (2005). *Assessment of existing offshore structures for life extension (Doctorial Thesis)*. Department of Mechanical and Structural Engineering and Material Sciences, University of Stavanger, Norway.
6. Galbraith, D. N., Sharp, J. V., Terry, E. (2005). Managing life extension in ageing offshore installations. *SPE Offshore Europe Oil and Gas Exhibition and Conference*, Aberdeen, UK.
7. Ersdal, G., Selnes, P. (2010). Life extension of ageing petroleum facilities offshore. *Society of Petroleum Engineers International Conference*, Rio de Janeiro, Brazil.
8. Solland, G., Sigurdsson, G., Ghosal, A. (2011). Life extension and assessment of existing offshore structures. *PE Project and Facilities Challenges Conference at METS*, Doha, Qatar.
9. Nezamian, A., Nicolson, R. J., Iosif, D. (2012). State of art in life extension of existing offshore structures. *International Conference on Offshore Mechanics and Arctic Engineering*, OMAE2012-83302, pp. 165–174. <https://doi.org/10.1115/OMAE2012-83302>

10. Ersdal, G., Sharp, J., Galbraith, D. (2014). Ageing accidents: Suggestion for a definition and examples from damaged platforms. *International Conference on Offshore Mechanics and Arctic Engineering*, OMAE2014-23674, V005T03A018. <https://doi.org/10.1115/OMAE2014-23674>
11. Ni, S., Tang, Y., Wang, G., Yang, L., Lei, B. et al. (2022). Risk identification and quantitative assessment method of offshore platform equipment. *Energy Reports*, 8, 7219–7229. <https://doi.org/10.1016/j.egy.2022.05.159>
12. Galbraith, D., Sharp, J. (2007). Recommendations for design life extension regulations. Doc. Id. POS-DK06-195-R02, Poseidon. <https://www.ptil.no/contentassets/24974571fd8442bea4c21d3679d93a8e/posdk06134r02revr02.pdf>
13. Stacey, A., Sharp, J. (2011). Ageing and life extension considerations in the integrity management of fixed and mobile offshore installations. *International Conference on Offshore Mechanics and Arctic Engineering*, pp. 49–65, OMAE2011-49090. <https://doi.org/10.1115/OMAE2011-49090>
14. Nezamian, A., Iqbal, K. (2015). Requalification and extension of service life and integrity requirements for offshore structures in Middle East. *International Petroleum Technology Conference*, IPTC-18540-MS. Doha, Qatar. <https://doi.org/10.2523/IPTC-18540-MS>
15. Potty, N. S., Akram, M. (2009). Structural integrity management for fixed offshore platforms in Malaysia. University Teknologi Petronas. <http://citeseerx.ist.psu.edu/viewdoc/download?doi=10.1.1.309.908&rep=rep1&type=pdf>
16. Banon, H., Bea, R., Bruen, F., Cornell, C., Krieger, W. et al. (1994). Assessing fitness for purpose of offshore platforms. I: Analytical methods and inspections. *Journal of Structural Engineering*, 120(12), 3595–3612. [https://doi.org/10.1061/\(ASCE\)0733-9445\(1994\)120:12\(3595\)](https://doi.org/10.1061/(ASCE)0733-9445(1994)120:12(3595))
17. Osmundsen, P., Tveterås, R. (2003). Decommissioning of petroleum installations—major policy issues. *Energy Policy*, 31(15), 1579–1588. [https://doi.org/10.1016/S0301-4215\(02\)00224-0](https://doi.org/10.1016/S0301-4215(02)00224-0)
18. Henrion, M., Bernstein, B., Swamy, S. (2015). A multi-attribute decision analysis for decommissioning offshore oil and gas platforms. *Integrated Environmental Assessment and Management*, 11(4), 594–609. <https://doi.org/10.1002/ieam.1693>
19. Rahman, M. J., Fawad, M., Jahren, J., Mondol, N. H. (2022). Top seal assessment of Drake Formation shales for CO₂ storage in the Horda Platform area, offshore Norway. *International Journal of Greenhouse Gas Control*, 119, 103700. <https://doi.org/10.1016/j.ijggc.2022.103700>
20. Mujeeb-Ahmed, M., Paik, J. K. (2021). Quantitative collision risk assessment of a fixed-type offshore platform with an offshore supply vessel. *Structures*, 29, 2139–2161. <https://doi.org/10.1016/j.istruc.2020.06.026>
21. Westlake, H., Puskar, F., O'Connor, P., Bucknell, J. (2006). The role of ultimate strength assessments in the Structural Integrity Management (SIM) of offshore structures. *Offshore Technology Conference*, Houston, Texas, USA.
22. Ghadimi, B., Taghikhany, T. (2021). Dynamic response assessment of an offshore jacket platform with semi-active fuzzy-based controller: A case study. *Ocean Engineering*, 238, 109747.
23. Yang, L., Ferrantelli, M., Hasan, F., Gregory, D., Jethvani, R. et al. (2021). American rescue plan and the effects of stimulus checks-New York City. <https://ssrn.com/abstract=3921162>
24. De, R. (1995). Risk analysis methodology for developing design and assessment criteria for fixed offshore structures. *Offshore Technology Conference*, Houston, Texas.
25. Krieger, W., Banon, H., Lloyd, J., De, R., Digre, K. et al. (1994). Process for assessment of existing platforms to determine their fitness for purpose. *Offshore Technology Conference*, Houston, Texas.
26. API (2020). Recommended practice 2A-WSD. Section 17: Assessment of existing platforms. API RP2A-WSD, 21st ed., supplement (R2020). https://www.api.org/~media/files/publications/whats%20new/2a-wsd_e22%20pa.pdf
27. DNV (1996). Guideline for offshore structural reliability analysis. In: *General part and applications to jackets*. Høvik (Norway): Det Norske Veritas.
28. Moan, T. (1998). Target levels for structural reliability and risk analysis of offshore structures. *Risk and Reliability in Marine Technology*, 1998, 351–368.
29. ISO (2020). ISO/DIS 13822, Bases for design of structures-assessment of existing structures. International Organization for Standardization.

30. ISO (2020). ISO 19920, Petroleum and natural gas industries-fixed steel offshore structures. International Organization for Standardization. <https://www.iso.org/standard/46556.html>
31. Syed Ahmad, S. Z. A., Abu Husain, M. K., Mohd Zaki, N. I., Mukhlis, N. A., Mat Soom, E. et al. (2021). Offshore structural reliability assessment by probabilistic procedures—A review. *Journal of Marine Science and Engineering*, 9(9), 998.
32. Wahab, M. M. A., Kurian, V. J., Liew, M. S., Kim, D. K. (2020). Condition assessment techniques for aged fixed-type offshore platforms considering decommissioning: A historical review. *Journal of Marine Science and Application*, 19(4), 584–614.
33. Hezarjaribi, M., Bahaari, M., Bagheri, V., Ebrahimian, H. (2013). Sensitivity analysis of jacket-type offshore platforms under extreme waves. *Journal of Constructional Steel Research*, 83, 147–155. <https://doi.org/10.1016/j.jcsr.2013.01.013>
34. Riboldi, L., Völler, S., Korpås, M., Nord, L. O. (2019). An integrated assessment of the environmental and economic impact of offshore oil platform electrification. *Energies*, 12(11), 2114. <https://doi.org/10.3390/en12112114>
35. Tian, X., Wang, Q., Liu, G., Liu, Y., Xie, Y. et al. (2019). Topology optimization design for offshore platform jacket structure. *Applied Ocean Research*, 84, 38–50. <https://doi.org/10.1016/j.apor.2019.01.003>
36. Sunder, S. S., Connor, J. (1981). Sensitivity analyses for steel jacket offshore platforms. *Applied Ocean Research*, 3(1), 13–26. [https://doi.org/10.1016/0141-1187\(81\)90081-X](https://doi.org/10.1016/0141-1187(81)90081-X)
37. Ayob, M., Kajuputra, A., Mukherjee, K., Wong, B. (2014). Global ultimate strength assessment of existing offshore jacket structures. *Offshore Technology Conference-Asia*, Kuala Lumpur, Malaysia.
38. Jimenez-Martinez, M. (2020). Fatigue of offshore structures: A review of statistical fatigue damage assessment for stochastic loadings. *International Journal of Fatigue*, 132, 105327. <https://doi.org/10.1016/j.ijfatigue.2019.105327>
39. Zhang, S., Yan, Y., Wang, P., Xu, Z., Yan, X. (2019). Sustainable maintainability management practices for offshore assets: A data-driven decision strategy. *Journal of Cleaner Production*, 237, 117730. <https://doi.org/10.1016/j.jclepro.2019.117730>
40. Ovunc, B. A. (1985). Soil-structure interaction and effect of axial force on the dynamics of offshore structures. *Computers & Structures*, 21(4), 629–637. [https://doi.org/10.1016/0045-7949\(85\)90141-5](https://doi.org/10.1016/0045-7949(85)90141-5)
41. HSE (1998). Dynamic push-over analysis of jacket structures. Technical Report OTO 98092 AME/37037B01/R/02.2), Health & Safety Executive, UK. Pre-pared by Mott MacDonald Oil Gas & Maritime Division; 1998.
42. Petronas (2019). PTS 34.19.00. 30, Design of fixed offshore structures (Working Stress Design). <https://www.petronas.com/>
43. MDP-A (2020). Metocean Criteria for Magtymguly Field, Document No. WW FS E ST 039 MET, July 2014, Revision 02.
44. MRC-A (2019). As Built Survey, DOC No. 415A-10-001, Rev B.
45. Systems, B. (2020). Structural analysis computer systems (SACS) software user guide manual, incorporated, release 10.2.0.1, 2015. <https://www.bentley.com/en/products/product-line/offshore-structural-analysis-software/sacs-offshore-structure>
46. Group, S. (2020). Ultimate strength of framed offshore structures (USFOS) software user guide manual, structural engineering marintek, Group 2020. https://www.usfos.com/manuals/usfos/users/documents/Usfos_UM_01.pdf
47. Petronas (2019). PTS 34.19.00. 10, Practice for the dynamic analysis of fixed offshore platforms for extreme storm conditions.
48. MDP-A (2018). Geotechnical Report, Engineering Assessments, MDP-A Platform, Pipelines and Calm Bouy, Block 1 Caspian Sea. Fugro Document No: N4563/03. Issue dated 8 September 2018.
49. ISO (1998). ISO 2394 General principles on reliability for structures. International Standardisation Organisation. <https://www.iso.org/standard/7289.html/>

50. ISO (2020). ISO 19900, Petroleum and natural gas industries–offshore structures–Part 1: General requirements. International Standardisation Organisation. <https://www.iso.org/standard/69761.html>
51. ISO (2020). ISO/DIS 19902, Design of fixed steel jackets. DIS Draft. International Standardisation Organisation. <https://www.iso.org/standard/65688.html>